IEICE Proceeding Series

Towards a photonic spiking neuron: excitability in a silicon-on-insulator microring.

T. Van Vaerenbergh, M. Fiers, K. Vandoorne, B. Schneider, J. Dambre, P. Bienstman

Vol. 1 pp. 767-770
Publication Date: 2014/03/17
Online ISSN: 2188-5079

2012 International Symposium on Nonlinear Theory and its Applications
NOLTA2012, Palma, Majorca, Spain, October 22-26, 2012

Towards a photonic spiking neuron: excitability in a silicon-on-insulator microring.

T. Van Vaerenbergh†, M. Fiers†, K. Vandoorne†, B. Schneider†, J. Dambre‡ and P. Bienstman†

†Photonics Research Group (INTEC), Ghent University - IMEC
‡Electronics and Information Systems (ELIS), Ghent University
Sint-Pietersnieuwstraat 41, B-9000 Ghent, Belgium
Email: thomas.vanvaerenbergh@intec.ugent.be

Abstract—For certain input power and wavelength settings, high Q-factor silicon-on-insulator rings self-pulsate. Thereby, they seem suited to emulate the behaviour of spiking neurons on a photonic chip. To gain insight in the possible excitation mechanisms a phase-plane analysis is needed. In this paper, we develop the theory needed to construct such phase portraits for a coupled mode theory description of the microring.
For some wavelengths, when changing the input power, the microring undergoes a subcritical Andronov-Hopf bifurcation at the self-pulsation onset. As a consequence the system is class II excitable.

1. Introduction

1.1. Photonic Reservoir Computing

On chip optical computation can outperform electronics in speed, bandwidth and power use, especially during the transfer of data between the different processing devices. However, nonlinear photonic components still do not reach the high yield standards of their electronic analogon, the transistor. One way of circumventing this problem, is shifting the computational paradigm. Instead of using a photonic version of the standard Von Neumann architecture, one can e.g. try to emulate neural networks on chip.
Moreover, if these neural networks are designed using the Reservoir Computing (RC) concept [1, 2], the specifications for the nonlinear components mimicking the neurons, are probably less stringent than for a photonic Von Neumann architecture. In RC the network is subdivided in a fixed, untrained recurrent network, the *reservoir*, and an easy trainable, mostly linear, feedforward *readout* layer. As the reservoir does not need to be trained and can be initialized in a random way, fabrication errors are potentially less problematic.
In Photonic Reservoir Computing (PRC) one tries to design photonic circuits which can serve as a hardware emulation of these kind of neural networks [3, 4, 5]. The topology restrictions on chip can hopefully be circumvented by the rich variety in dynamics of nonlinear optical components. Most attention of the current research is now on the choice of these nonlinear components.

1.2. Silicon On Insulator microrings

In this paper, we will focus on a simple Silicon On Insulator (SOI) microring. When the wavelength of the input signal is close to the resonance of the cavity, for high enough input powers, due to heating and the thermo-optic effect, bistable behaviour is obtained. High Q-factor rings can even start to self-pulsate, as light will generate free carriers which will change the refractive index [6]. As the microrings can be bistable and self-pulsate they seem suited to imitate the behaviour of spiking neurons.
In literature the mechanism behind this excitability in microrings, microdisks and similar passive cavities is often explained using Coupled Mode Theory (CMT). Timedomain simulations in this formalism show a good correspondence with experiment [7, 8]. Moreover, the steady-state equations are still analytically solvable, both for varying power and wavelength of the input light. For SOI microdisks no hysteresis in the threshold of the input wavelength for the onset of oscillations is found, which indicates a super-critical Andronov-Hopf bifurcation[1] [8].
Moreover, the CMT-equations can be rewritten in the mean-field model used in [9]. Using the steady-state curves and corresponding 2D projections of nullclines of this model, the class II excitability of a 2D Indium Phosphide (InP) Photonic Crystal (PhC) can be explained [9]. There as well, a sweep of the input wavelength indicates a Andronov-Hopf bifurcation, the observed excitability of the PhC indicates that it is sub-critical. Similar behaviour appears in PhC nanocavities [10].

2. Microring: nonlinear behaviour

Optical bistability and self-pulsation in a SOI-microring has experimentally been demonstrated [6]. The bistability is caused by the thermo-optic effect in which absorption heats the microring cavity resulting in a redshift in the

[1] Although the author of that paper indicates that further examination might be worthwhile.

resonance wavelength. In bulk Silicon two photon absorption (TPA) generates free carriers. These free carriers are able to absorb light by free carrier absorption (FCA). In addition, the presence of free carriers causes a blueshift in the wavelength by free carrier dispersion (FCD). In SOI microrings also (linear) surface state absorption at the Silicon-Silica interface is present [6].

When the backscattering in the microring is neglected, the dynamics of the ring can be described in CMT with one complex variable (the mode amplitude $a = |a|e^{j\phi}$, with $|a|^2$ the energy in the cavity and ϕ the phase), and two real variables (the mode-averaged temperature difference with the surroundings ΔT and the amount of free carriers N). In this paper, we study an all-pass filter with one input: a single ring coupled with only one bus waveguide. The CMT-equations are then [8]:

$$\frac{\mathrm{d}a}{\mathrm{d}t} = \left[j\left(\omega_r + \delta\omega_{nl} - \omega\right) - \frac{\gamma_{loss}}{2}\right] a + \kappa s_{in}, \quad (1)$$

$$\frac{\mathrm{d}\Delta T}{\mathrm{d}t} = -\frac{\Delta T}{\tau_{th}} + \frac{\Gamma_{th}\gamma_{abs}|a|^2}{\rho_{Si}c_{p,Si}V_{th}}, \quad (2)$$

$$\frac{\mathrm{d}N}{\mathrm{d}t} = -\frac{N}{\tau_{fc}} + \frac{\Gamma_{FCA}\beta_{Si}c^2|a|^4}{2\hbar\omega V_{FCA}^2 n_g^2}, \quad (3)$$

$$s_{out} = e^{j\phi_c}s_{in} + \kappa a, \quad (4)$$

with s_{in} the amplitude of the input light (input power $P_{in} = |s_{in}|^2$), s_{out} the amplitude of the output light (output power $P_{out} = |s_{out}|^2$), ϕ_c the phase propagation in the bus waveguide, κ the coupling from waveguide to ring, $\omega_r = \frac{2\pi c}{\lambda_r}$ the resonance frequency of the cavity and $\omega = \frac{2\pi c}{\lambda}$ the frequency of the input light. τ_{th} and τ_{fc} are the relaxation times for resp. the temperature and the free carriers. β_{Si} is the constant governing TPA, $c_{p,Si}$ the thermal capacity, ρ_{Si} the density of Silicon and n_g is the group index. We also use the effective volumes $V...$ and confinements $\Gamma...$ defined in [8]. In Eqs. 1 and 2 γ_{loss} and γ_{abs} are resp. the total loss and absorption loss in the cavity, with:

$$\gamma_{loss} = \gamma_{coup} + \gamma_{rad} + \gamma_{abs}, \quad (5)$$

where we have introduced the coupling loss into the waveguide γ_{coup} (with $\kappa = j\sqrt{\frac{\gamma_{coup}}{2}}e^{j\phi_c}$) and the radiation loss γ_{rad}. In the ring we have absorption by linear surface absorption, TPA and FCA :

$$\gamma_{abs} = \gamma_{abs,lin} + \Gamma_{TPA}\frac{\beta_{Si}c^2|a|^2}{n_g^2 V_{TPA}} + \Gamma_{FCA}\frac{\sigma_{Si}c}{n_g}N, \quad (6)$$

σ_{Si} is the absorption cross section of FCA and $\gamma_{abs,lin}$ the linear absorption constant. In [6] one measures $\eta_{lin} = \frac{\gamma_{abs,lin}}{\gamma_{abs,lin}+\gamma_{rad}} \approx 0.4$, we use this value throughout the paper. The thermo-optic effect and FCD both cause a shift in the resonance frequency ω_r. In this case, the Kerr-effect is negligible. This gives in first order perturbation theory:

$$\frac{\Delta\omega_{nl}}{\omega_r} = -\frac{1}{n_{Si}}\left(\frac{\mathrm{d}n_{Si}}{\mathrm{d}T}\Delta T + \frac{\mathrm{d}n_{Si}}{\mathrm{d}N}N\right), \quad (7)$$

with n_{Si} the refractive index of bulk Silicon. Setting the derivatives to zero in Eqs. 1-3 results in the steady-state equations. These can be solved analytically. In very high Q-rings TPA generates enough free carriers to make FCD prominent for high enough input powers. We will illustrate the concepts of this paper for such a SOI $4\,\mu$m-radius microring with $540\,\mathrm{nm} \times 220\,\mathrm{nm}$ cross section waveguides. This ring has a resonance width $\lambda_{3dB} = 25\,\mathrm{pm}$ at the resonance wavelength $\lambda_r = 1552.770\,\mathrm{nm}$. We consider a critically coupled ring with $\gamma_{coup} = \gamma_{abs,lin} + \gamma_{rad}$.

The analytic steady-state $P_{out}(P_{in})$-curve is bistable, due

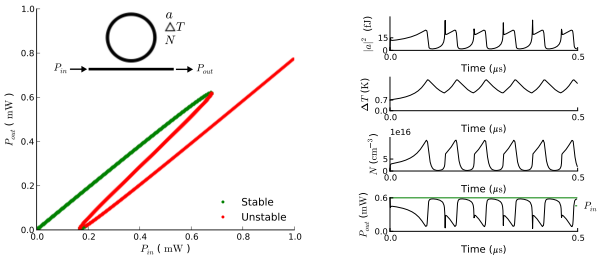

Figure 1: For detuning $\lambda - \lambda_r = 62\,\mathrm{pm}$, $P_{out}(P_{in})$ is bistable (left side figure), for P_{in} higher then $\approx 190\,\mu$W the lower P_{out}-branch gets unstable, which is an indication of self-pulsation. For $P_{in} = 600\,\mu$W and $(a, \Delta T, N)(t{=}0){=}(0, 0.7, 0)$ this gives the self-pulsation timetrace on the right.

to thermal and free carrier nonlinearities (Fig. 1, left). As the light energy both heats up the cavity and generates free carriers, and the thermo-optic and FCD have an opposite influence on the effective resonance wavelength (and thus the amount of light coupled into the cavity), self-pulsation is possible with a mostly asymmetric pulse shape, caused by the difference in timescale between the fast free carrier generation and absorption of optical power and the slow relaxation of the temperature in the cavity. For higher input powers there are no stable fixed points and the ring will always self-pulsate. For lower input powers there can be two stable fixpoints in combination with an unstable one (if $P_{in} = 167 - 191\,\mu$W) or one stable fixpoint together with a stable limit cycle and two unstable fixpoints (if $P_{in} > 191\,\mu$W).

3. Phase-plane analysis

To gain more insight in the bifurcation mechanism we now project the time-traces for a given input power and wavelength on the (ΔT,N)-plane. Moreover, we calculate the $d(\Delta T, N)/dt = 0$, $d(\Delta T, a)/dt = 0$ and $d(N, a)/dt = 0$ nullclines. Where the three curves intersect we have steady-state points. $d(N, a)/dt = 0$ and $d(\Delta T, a)/dt = 0$ only intersect in the (ΔT,N)-plane in those fixpoints (Fig. 2). This can be intuitively understood

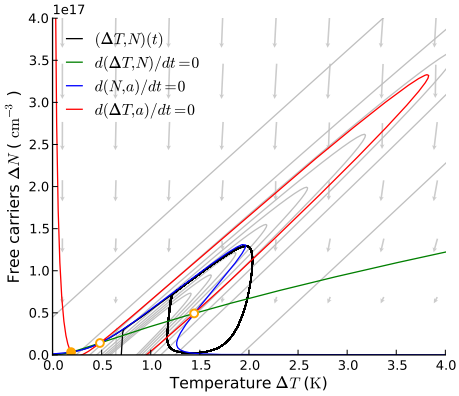

Figure 2: On the phase portrait for $P_{in} = 600\,\mu$W and a 62 pm detuning, the $d(N,a)/dt = 0$, $d(\Delta T,a)/dt = 0$ nullclines only intersect at the three fixed points (orange circles). In correspondence with Fig. 1 two of those fixpoints are unstables (open circle), while one is stable (filled circle). The example timetrace from Fig. 1 (black line) clearly follows both the $d(\Delta T,N)/dt$ directions on the $da/dt = 0$-surface (grey arrows) and the corresponding direction changes indicated by the nullclines. Moreover, (grey) contour lines of $da/dt = 0$ for $|a|^2 = 1\,\mathrm{fJ} - 31\,\mathrm{fJ}$ are elliptic and do not overlap.

by considering the projection of the $da/dt = 0$ surface on the (ΔT,N)-plane. It can be proven that the contour line for a given $|a|$-value is an ellipse. The orientation of the principal axes is independent of $|a|$. However, the center of this ellipse and the global scaling factor of the axes both are monotically $|a|$-dependent, the size of the ellipse e.g. shrinks for higher $|a|^2$. In the case of our ring, this dependence is in such a way that ellipses corresponding with different $|a|$-values do not overlap. This has as a consequence that the projection of the $da/dt = 0$ surface on the (ΔT,N)-plane is a bijection. Both $d(\Delta T,a)/dt = 0$ and $d(\Delta N,a)/dt = 0$ lie on the $da/dt = 0$ surface and only intersect in the fixpoints, the intersections of their projections thus uniquely correspond with those fixpoints. Although we do not yet have a general proof that this unique correspondence is always valid, we hereby constructed a visual manner to check this: as long as the ellipses corresponding with different $|a|$-values do not overlap we can identify the fixpoints only by looking at the intersections of $d(\Delta N,a)/dt = 0$ and $d(\Delta T,a)/dt = 0$ in the (ΔT,N)-plane.

Both the temperature time constant ($\tau_{th} = 65\,\mathrm{ns}$) and the free carrier relaxation time ($\tau_{fc} = 5.3\,\mathrm{ns}$) are bigger than the time constants governing the dynamics of the light ($\tau_{abs,lin} = \tau_{coup} = 2/\gamma_{coup} = 205\,ps$, and the detuning of the light corresponds with a time constant of the same order of magnitude). After a very short transient period $\approx 100\,ps$ $da/dt \approx 0$, the (a,ΔT,N)(t) solutions are then converged to the $da/dt = 0$ surface. We can thus use the projections of the $d(\Delta N,a)/dt = 0$ and $d(\Delta T,a)/dt = 0$ nullclines to the (ΔT,N)-plane to do standard 2D phase-plane analysis.

4. Bifurcation analysis

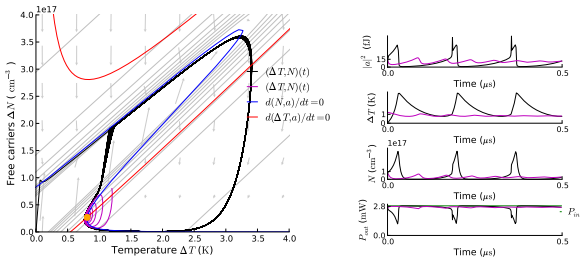

Figure 3: For some input powers and wavelength settings the limit cycle encloses a stable fixpoint in the $(\Delta T, N)$ phase-plane. This indicates a subcritical Andronov-Hopf bifurcation. We illustrate this here for $P_{in} = 2.85\,\mathrm{mW}$ and $\delta\lambda = -16\,\mathrm{pm}$. Depending on the initial conditions, the trajectory will converge to the limit cycle (black curve $(\Delta T, N) = (0, 0)$) or to the fixpoint (magenta curve $(\Delta T, N) = (1.2\,\mathrm{K}, 8\mathrm{e}16\,\mathrm{cm}^{-3})$).

For a given input power the microring can have one, two or three fixpoints (Fig. 2). The microring undergoes a saddle-node bifurcation if it has two fixpoints. If it has three fixpoints, at least one (at low $|a|$) is stable.When two of the three fixpoints are unstable, there is a stable limit cycle around the high $|a|$-fixpoint. The middle fixpoint will always be unstable, and is a saddle-node. It has an unstable manifold which ends at the low $|a|$ stable fixpoint and, if there is one, at the upper limit cycle, or else, at the high $|a|$ stable fixpoint. A stable manifold or separatrix divides the basins of attraction of the lower fixpoint and the higher $|a|$ fixpoint/limit cycle. If there is only one fixpoint and it is unstable, then there is a stable limit cycle around it.

For some wavelengths, the onset of oscillation shows hysteresis in the input power, which is a sign of a subcritical Andronov-Hopf bifurcation. Given the previous ring parameters, this happens if the input light is blue-detuned, where there is no bistability. The basin of attraction of the stable fixpoint centered in the limit cycle is determined by an unstable limit cycle in-between the stable limit cycle and this fixpoint. This can be proved explicitly with time traces for e.g. $P_{in} = 2.85\,mW$ at a $\delta\lambda = -16\,\mathrm{pm}$ detuning, where we have one stable fixpoints and a stable limit cycle. By choosing carefully the initial conditions within the region defined by the limit cycle on the $da/dt = 0$ surface we can end in the central fixpoint or in the limit

cycle (Fig. 3). The basin of attraction of the stable fixpoint centered in the limit cycle is determined by an unstable limit cycle in-between the stable limit cycle and this fixpoint. The stable and unstable limit cycle annihilate in a fold limit cycle bifurcation for lower input powers.

5. Excitability

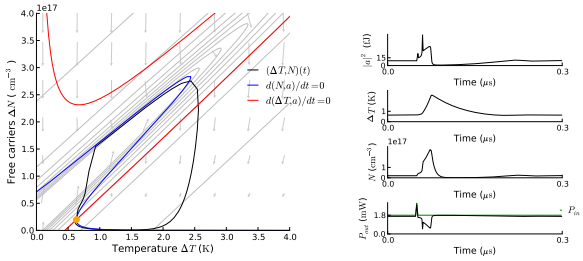

Figure 4: A temporary increase of $P_{in} = 1.8\,\mathrm{mW}$ at $\delta\lambda = -16\,\mathrm{pm}$ to $2.9\,\mathrm{mW}$, during $2\,\mathrm{ns}$, triggers an excitation. Although for this input power no limit cycle is present, the excitation can be seen as a reminiscent of the nearby limit cycle from Fig. 3.

In the wavelength region where the self-pulsation hysteresis is present the microring is excitable if the input power is below, but close to, the fold limit cycle bifurcation (Fig. 5, with a $T_{tr} = 2\,\mathrm{ns}$ long power increase as perturbation). For these input settings a small perturbation will kick the ring out of his rest state, into a 'ghost' of a limit cycle pulse, whereafter the system will return to the initial rest state. In this power region there does not yet exist a stable limit cycle, but the phase plane incorporates already similar dynamics, as we are close to the bifurcation point. This is illustrated by the similarity between the pulse-trajectory in the phase plane in Fig. 5 and Fig. 3. This corresponds with class II excitability [11].

6. Conclusions

A high Q all-pass microring self-pulsates for certain input power and wavelength settings, which can be described with CMT, using the complex mode amplitude a of the light in the cavity, the temperature difference with the surrounding ΔT and the amount of free carriers N as variables. Neglecting the fast energy and phase dynamics of the light allows a 2D phase-plane analysis.
For some wavelengths, when changing the input power, the microring undergoes a subcritical Andronov-Hopf bifurcation at the self-pulsation onset. As a consequence the system shows the signature of class II excitability. This thorough understanding of the possible excitability mechanisms will allow a correct characterization of the computational properties of a microring, within a photonic spiking neuron usage.

Acknowledgments

This work is supported by the interuniversity attraction pole (IAP) Photonics@be of the Belgian Science Policy Office and the ERC NaResCo Starting grant. T. Van Vaerenbergh is supported by the Flemish Research Foundation (FWO-Vlaanderen) for a PhD Grant. M. Fiers acknowledges the Special Research Fund of Ghent University.

References

[1] W. Maass, et al., "Real-time computing without stable states: A new framework for neural computation based on perturbations," Neural Computation **14**, 2531–2560 (2002).

[2] H. Jaeger, "Harnessing nonlinearity: Predicting chaotic systems and saving energy in wireless communication," Science **304**, 78–80 (2004).

[3] K. Vandoorne, et al., "Parallel reservoir computing using optical amplifiers," IEEE transactions on neural networks **22**, 1469–1481 (2011).

[4] Y. Paquot, et al., and S. Massar, "Optoelectronic reservoir computing." Scientific reports **2**, 287 (2012).

[5] L. Larger, et al., "Photonic information processing beyond Turing: an optoelectronic implementation of reservoir computing," Opt. Exp. **20**, 3241 (2012).

[6] G. Priem, et al., "Optical bistability and pulsating behaviour in Silicon-On-Insulator ring resonator structures." Opt. exp. **13**, 9623–8 (2005).

[7] W. H. P. Pernice, et al., "Time-domain measurement of optical transport in silicon micro-ring resonators." Opt. exp. **18**, 18438–52 (2010).

[8] T. J. Johnson, et al., "Self-induced optical modulation of the transmission through a high-Q silicon microdisk resonator." Opt. exp. **14**, 817–31 (2006).

[9] A. Yacomotti, et al., "Fast Thermo-Optical Excitability in a Two-Dimensional Photonic Crystal," Phys. Rev. Lett. **97**, 6–9 (2006).

[10] M. Brunstein, et al., "Excitability and self-pulsing in a photonic crystal nanocavity," Phys. Rev. A **85**, 1–5 (2012).

[11] E. M. Izhikevich, *Dynamical Systems in Neuroscience: The Geometry of Excitability and Bursting (Computational Neuroscience)* (The MIT Press, 2006), 1st ed.